Dispersion engineered $Ge_{11.5}As_{24}Se_{64.5}$ nanowire for supercontinuum generation: A parametric study

M. R. Karim,[1,*] B. M. A. Rahman,[1] and G. P. Agrawal[2]

[1] *School of Engineering and Mathematical Sciences, City University London, Northampton Square, London, EC1V 0HB, UK*

[2] *The Institute of Optics, University of Rochester, Rochester, New York, 14627, USA*

[*] *mohammad.karim.2@city.ac.uk*

Abstract: A promising design of $Ge_{11.5}As_{24}Se_{64.5}$ nanowires for supercontinuum generation is proposed through numerical simulations. It can be used for generating a supercontinuum with 1300-nm bandwidth. The dispersion parameters upto eighth-order are obtained by calculating the effective mode index with the finite-element method. We have investigated dispersion curves for a number of nanowire geometries. Through dispersion engineering and by varying dimensions of the nanowires we have identified a promising structure that shows possibility of realizing a wideband supercontinuum. We have found significant variations in its bandwidth with the inclusion of higher-order dispersion coefficients and indicated the possibility of obtaining spurious results if the adequate number of dispersion coefficients is not considered. To confirm the accuracy of dispersion coefficients obtained through numerical computations, we have shown that a data-fitting procedure based on the Taylor series expansion provides good agreement with the actual group velocity dispersion curve obtained by using a full-vectorial finite-element mode-solver.

OCIS codes: (000.4430) Numerical approximation and analysis; (190.4390) Nonlinear optics, integrated optics; (230.7370) Dispersion; (320.6629) Supercontinuum generation; (130.2755) Glass waveguides.

References and links

1. J. M. Dudley, G. Genty, and S. Coen, "Supercontinuum generation in photonic crystal fiber," Rev. Mod. Phys. **78**, 1135–1184 (2006).
2. G. P. Agrawal, *Nonlinear Fiber Optics 5th ed.* (Academic press, San Diego, California, 2013).
3. J. Hu, C. R. Menyuk, L. B. Shaw, J. S. Sanghera, and I. D. Aggarwal, "Maximizing the bandwidth of supercontinuum generation in As_2Se_3 chalcogenide fibers," Opt. Express **18**(3), 6722–6739 (2010).
4. L. Yin, Q. Lin, G. P. Agrawal, "Soliton fission and supercontinuum generation in silicon waveguides," Opt. Lett. **32**(4), 391–393 (2007).
5. I. W. Hsieh, X. G. Chen, J. I. Dadap, N. C. Panoiu, and R. M. Osgood, Jr., "Ultrafast-pulse self-phase modulation and third-order dispersion in Si photonic wire-waveguides," Opt. Express **14**(25), 12380–12387 (2006).
6. I. W. Hsieh, X. G. Chen, X. P. Liu, J. I. Dadap, N. C. Panoiu, C. Y. Chou, F. N. Xia, W. M. Green, Y. A. Vlasov, and R. M. Osgood, Jr., "Supercontinuum generation in silicon photonic wires," Opt. Express **15**(23), 15242–15249 (2007).
7. M. R. E. Lamont, B. Luther-Davies, D. Y. Choi, S. Madden, and B. J. Eggleton, "Supercontinuum generation in dispersion engineered highly nonlinear ($\gamma = 10$ /W/m) As_2S_3 chalcogenide planar waveguide," Opt. Express **16**(19), 14938–14944 (2008).

8. B. J. Eggleton, B. Luther-Davies, and K. Richardson, "Chalcogenide photonics," Nat. Photonics **5**, 141–148 (2011).
9. D. Yeom, E. C. Mägi, M. R. E. Lamont, M. A. F. Roelens, L. Fu, and B. J. Eggleton, "Low-threshold supercontinuum generation in highly nonlinear chalcogenide nanowires," Opt. Lett. **33**(7), 660–662 (2008).
10. D. D. Hudson, S. A. Dekker, E. C. Mägi, A. C. Judge, S. D. Jackson, E. Li, J. S. Sanghera, L. B. Shaw, I. D. Aggarwal, and B. J. Eggleton, "Octave spanning supercontinuum in an As_2S_3 taper using ultralow pump pulse energy," Opt. Lett. **36**(7), 1122–1124 (2011).
11. D. D. Hudson, E. C. Mägi, A. C. Judge, S. A. Dekker, and B. J. Eggleton, "Highly nonlinera chalcogenide glass micro/nanofiber devices: Design, theory, and octave-spanning spectral generation," Opt. Commun. **285**, 4660–4669 (2012).
12. I. D. Aggarwal and J. S. Sanghera, "Development and applications of chalcogenide glass optical fibers at NRL," J. Optoelectron. Adv. Mater. **4**(3), 665–678 (2002).
13. X. Gai, S. Madden, D. Y. Choi, D. Bulla, and B. Luther-Davies, "Dispersion engineered $Ge_{11.5}As_{24}Se_{64.5}$ nanowires with a nonlinear parameter of 136 $W^{-1}m^{-1}$ at 1550 nm," Opt. Express **18**(18), 18866–18874 (2010).
14. X. Gai, T. Han, A. Prasad, S. Madden, D. Y. Choi, R. Wang, D. Bulla, and B. Luther-Davies, "Progress in optical waveguides fabricated from chalcogenide glasses," Opt. Express **18**(25), 26635–26646 (2010).
15. D. D. Hudson, M. Baudisch, D. Werdehausen, B. J. Eggleton, and J. Biegert, "1.9 octave supercontinuum generation in a As_2S_3 step-index fiber driven by mid-IR OPCPA," Opt. Lett. **39**(19), 5752–5755 (2014).
16. P. Ma, D. Y. Choi, Y. Yu, X. Gia, Z. Yang, S. Debbarma, S. Madden, and B. Luther-Davies, "Low-loss chalcogenide waveguides for chemical sensing in the mid-infrared," Opt. Express **21**(24), 29927–29937 (2013).
17. C. Choudhari, M. Liao, T. Suzuki, and Y. Ohishi, "Chalcogenide core tellurite cladding composite microstructured fiber for nonlinear applications," J. Lightwave Technol. **30**(13), 2069–2076, (2012).
18. M. R. E. Lamont, C. M. Sterke, and B. J. Eggleton, "Dispersion engineering of highly nonlinear As_2S_3 waveguides for parametric gain and wavelength conversion," Opt. Express **15**(15), 9458–9463 (2007).
19. F. Luan, M. D. Pelusi, M. R. E. Lamont, D. Y. Choi, S. Madden, B. Luther-Davies, and B. J. Eggleton, "Dispersion engineered As_2S_3 planar waveguides for broadband four-wave mixing based wavelength conversion of 49 Gb/s signals," Opt. Express **17**(5), 3514–3520 (2009).
20. S. J. Madden, D. Y. Choi, D. A. Bulla, A. V. Rode, B. Luther-Davies, V. G. Ta'eed, M. D. Pelusi, and B. J. Eggleton, "Long, low loss etched As_2S_3 chalcogenide for all-optical signal regeneration," Opt. Express **15**(22), 14414–14421 (2007).
21. B. M. A. Rahman and J. B. Davies, "Vector-*H* finite element soluion of GaAs/GaAlAs rib waveguides," Proc. IEE **132**(6), 349–353 (1985).
22. N. Granzow, M.A. Schmidt, W. Chang, L. Wang, Q. Coulombier, J. Troles, P. Toupin, I. Hartl, K. F. Lee, M. E. Fermann, L. Wondraczek, and P. St. J. Russell, "Mid-infrared supercontinuum generation in As_2S_3 "nano-spike" step index waveguide," Opt. Express **21**(9), 10969–10977 (2013).
23. B. M. A. Rahman and J. B. Davies, "Finite-element solution of integrated optical waveguides," J. Lightwave Technol. **2**(5), 682–688, (1984).
24. D. V. Skryabin, F. Laun, J. C. Knight, and P. St. J. Russel, "Soliton self-frequency shift cancellation in photonic crystal fibers," Science, **301**, 1705–1708 (2003).
25. F. Biancalana, D. V. Skryabin, and A. V. Yulin, "Theory of the soliton self-frequency shift compensation by resonant radiation in photonic crystal fibers," Physical Review E, **70**, 016615 (2004).
26. W. Gao, M. E. Amraoui, M. Liao, H. Kawashima, Z. Duan, D. Deng, T. Cheng, T. Suzuki, Y. Messaddeq, and Y. Ohishi, "Mid-infrared supecontinuum generation in a suspended-core As_2S_3 chalcogenide microstructured optical fiber," Opt. Express **21**(8), 9573–9583 (2013).
27. J. M. Dudley and J. R. Taylor, *Supercontinuum Generation in Optical Fibers* (Cambridge University, 2010).
28. N. Granzow, S. P. Stark, M. A. Schmidt, A. S. Tverjanovich, L. Wondraczek, and P. St. J. Russell, "Supercontinuum generation in chalcogenide-slica step-index fibers," Opt. Express **19**(21), 21003–21010 (2011).

1. Introduction

Supercontinuum (SC) generation using nonlinear effects in optical waveguides has been a topic of considerable interest in nonlinear optics over the last decade as its use provides an optical source with properties such as large bandwidth, brightness, high coherence, and potential compactness. Broadband supercontinuum sources have found many applications in the field of spectroscopy, bio-imaging, pulse compression, optical coherence tomography, and high precision frequency metrology [1]. Highly nonlinear waveguides in combination with a mode-locked laser are used to produce such a source through the process called SC generation. SC generation relies on the interplay of various nonlinear effects such as self-phase modulation, cross-phase modulation, soliton dynamics, Raman scattering, and four-wave mixing, and it re-

quires an optical waveguide with suitably designed group velocity dispersion (GVD), including a zero-dispersion wavelength (ZDW) close to the pump wavelength [2]. To generate a SC with a large bandwidth ranging from ultra-violet (UV) to mid-infrared (MIR) regions with high brightness, numerous efforts have focused on fused silica fibers. However, the intrinsic transmission window of fused silica makes SC expansion beyond 2.2 μm a challenging task [3]. Silicon (Si) offers a high Kerr nonlinearity and is attractive for generating SC using Slicon-on-insulator (SOI) nanowires [4–6]. Although Si has low losses in the near infrared, it has some disadvantage in the telecommunication band centered at 1550 nm where it is affected by two-photon absorption (TPA) and free-carrier absorption (FCA), both of which clamp spectral broadening of SC and limit the achievable bandwidth [7].

In recent years chalcogenide glasses are emerging as promising nonlinear materials in the infrared (IR) region extending from 1 to 5 μm. Such glasses have a number of unique properties which make them attractive for fabricating planar optical waveguides, including low nonlinear absorption, low TPA, no FCA, and fast response time because of the absence of free-carrier effects [8–11]. Their high refractive index (2-3) and broad infrared transparency (0.6-15 μm) [12] make them attractive for waveguide fabrication in the field of telecommunications, optical sensing, and MIR sciences. A major advantage of the chalcogenide glasses is their large ultra-fast third-order nonlinearity. These materials are highly suitable not only for nonlinear applications but also for making compact active and passive devices in the MIR region [13–15]. Moreover a specific chalcogenide glass $Ge_{11.5}As_{24}Se_{64.5}$ has excellent film-forming properties and high thermal and optical stability under intense illumination [16]. Motivated by such useful properties, interest has grown in designing and optimizing planar waveguides made from $Ge_{11.5}As_{24}Se_{64.5}$ glass for SC generation, parametric amplification, wavelength conversion, and signal regeneration [17–20].

In this paper, numerical simulations are used for demonstrating broadband SC generation in a highly nonlinear nanowire made from $Ge_{11.5}As_{24}Se_{64.5}$ chalcogenide glass. The propagation loss (α) and Kerr nonlinear refractive index (n_2) were taken to be 3.2 dB/cm and 8.6×10^{-18} m^2/W, respectively for the fundamental transverse electric (TE) mode [14]. Various geometries of chalcogenide nanowires with optimized waveguide dimensions are investigated to tailor dispersion and to obtain the ZDW close to the pump wavelength. We carry out simulations for different promising nanowire structures and proposed an optimized design for SC generation among these structures. Using our optimized nanowire, a broadband SC can be generated extending from 1200 nm to around 2500 nm by employing 1550 nm pump pulses of 50 fs (FWHM) duration with 25 W peak power. In all simulations the waveguide length is 18 mm. We also analyzed the effect of higher-order dispersion coefficients, upto eighth-order (β_8) term, on SC and found significant changes to occur in the SC bandwidth when higher-order dispersion terms are included in numerical simulations.

2. Theory

The structure of the $Ge_{11.5}As_{24}Se_{64.5}$ nanowire is shown in Fig. 1 as an inset. The wavelength-dependent linear refractive index n of $Ge_{11.5}As_{24}Se_{64.5}$ glass over the entire wavelength range used in the simulation are given by the Sellmeier equation [16],

$$n^2(\lambda) = 1 + \frac{5.78525\lambda^2}{\lambda^2 - 0.28795^2} + \frac{0.39705\lambda^2}{\lambda^2 - 30.39338^2}, \tag{1}$$

Here λ is the wavelength in micrometers.

Dispersion of the waveguide plays an important role in determining the supercontinuum spectrum. Ideally dispersion near the pump wavelength should be small in magnitude as well as relatively flat in nature [26]. Chalcogenide glasses generally have smaller material disper-

sion than silicon. However, to obtain the ZDW close to the pump wavelength, relatively larger waveguide dispersion is required to offset the material dispersion, resulting in a waveguide that supports more than one mode. To reduce higher-order modes, a polymer cladding with a refractive index value of 1.51 is often used in place of air cladding [13] as it reduces the index contrast between the core and cladding of the nanowire. We use a finite element (FE) based mode-solver to calculate the effective index (n_{eff}) as a function of frequency, which is subsequently used for numerically calculating GVD as well as all other higher-order dispersion parameters. Spectral broadening of a SC mainly depends on these dispersion parameters and the nonlinear coefficient, γ, which in turn depends on the nonlinear refractive index of the material, n_2 and effective mode area of the waveguide. Optimized mode area, A_{eff} can be obtained by using our FE mode-solver [23] and using this A_{eff} a relatively large nonlinear co-efficient can be realized [3].

The FE approach used here is based on the vector-**H**-field formulation, since it is one of the most accurate and numerically efficient approaches to obtain the modal field profiles and mode propagation constants $\beta(\omega)$ of various quasi-TE and quasi-TM modes. The full-vectorial formulation is based on the minimization of the full **H**-field energy functional [23],

$$\omega^2 = \frac{\iint \left[(\nabla \times \mathbf{H})^*.\hat{\varepsilon}^{-1}(\nabla \times \mathbf{H}) + p(\nabla.\mathbf{H})^*(\nabla.\mathbf{H})\right] dxdy}{\iint \mathbf{H}^*.\hat{\mu}\mathbf{H} dxdy}, \tag{2}$$

where **H** is the full-vectorial magnetic field, * denotes a complex conjugate and transpose, ω^2 is the eigenvalue (ω being the angular frequency), p is a weighting factor for the penalty term to eliminate spurious modes and $\hat{\varepsilon}$ and $\hat{\mu}$ are the permittivity and permeability tensors, respectively. The two-dimensional cross-section of the waveguide is discretized by using a large number of triangular elements. All three components of the magnetic fields can be represented as piece-wise polynomials within the elements. With a proper choice of waveguide discretization we can accurately calculate the energy functional by integrating it over each element.

To study supercontiuum generation, simulations were performed using a generalized nonlinear Schrödinger equation (GNLSE) for the slowly varying envelope of the pulse [4, 13]:

$$\frac{\partial}{\partial z}A(z,T) = -\frac{\alpha}{2}A + \sum_{m\geq 2}\frac{i^{m+1}}{m!}\beta_m\frac{\partial^m A}{\partial T^m} + i\left(\gamma + i\frac{\alpha_2}{2A_{eff}}\right)\left(1+\frac{i}{\omega_0}\frac{\partial}{\partial T}\right) \times \left(A(z,T)\int_{-\infty}^{\infty} R(T)\mid A(z,T-T')\mid^2 dT'\right), \tag{3}$$

where A is the electrical field amplitude, α is the linear propagation loss of the waveguide, $\beta_m(\omega) = \frac{d^m\beta}{d\omega^m}\big|_{\omega=\omega_0}$ ($m \geq 2$) is the m$^{\text{th}}$ order dispersion parameter, and $T = t - \frac{z}{v_g}$ is the retarded time frame moving with the group velocity $v_g = \frac{1}{\beta_1(\omega_0)}$ at the pump frequency ω_0. The nonlinear coefficient is $\gamma = \frac{n_2\omega_0}{cA_{\text{eff}}(\omega_0)}$, where n_2 is the nonlinear refractive index and c is the speed of light in vacuum, $A_{\text{eff}}(\omega_0)$ is the effective area of the mode at the pump frequency ω_0, and $\alpha_2 = 9.3\times10^{-14}$ m/W is the two-photon absorption coefficient [13]. Finally the material response function includes both the instantaneous electronic response (Kerr type) and the delayed Raman response and has the form

$$R(t) = (1-f_R)\delta(t) + f_R h_R(t), \tag{4}$$

$$h_R(t) = \frac{\tau_1^2+\tau_2^2}{\tau_1\tau_2^2}\exp\left(-\frac{t}{\tau_2}\right)\sin\left(\frac{t}{\tau_1}\right), \tag{5}$$

where $f_R = 0.031$, $\tau_1 = 15.5$ fs, and $\tau_2 = 230.5$ fs for our Chalcogenide material [22, 26, 28].

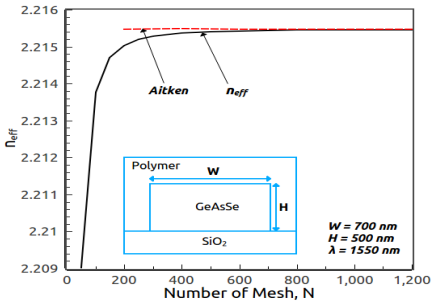

Fig. 1. Variation of n_{eff} of the fundamental quasi-TE mode with the mesh size and improvement realized with the Aitken extrapolation technique. Geometry of nanowire is shown as an inset.

3. Numerical results

Before performing supercontinuum simulations, accuracy of the finite-element modal solutions is tested. It is well-known that accuracy of numerical solutions depends on several discretization parameters. For our optical waveguides, solution accuracy depends on the finite number of elements used to characterize it. From the FE modal solution we have obtained the propagation constant $\beta(\omega)$ which was used for calculating $n_{\text{eff}} = \lambda\beta(\omega)/2\pi$ of the waveguide. As the dispersion of waveguide depends on n_{eff} which varies with λ, the accuracy of GVD also required testing as well as all higher-order dispersion coefficients calculated from it. Variation of the effective index, n_{eff} with the number of mesh divisions N used is shown in Fig. 1 by a solid black line for the fundamental quasi-TE mode of a waveguide designed with the width and thickness, $W = 700$ nm, $H = 500$ nm and the operating wavelength of 1550 nm. The same value of N was used in both transverse directions. It can be observed that, as N increases, n_{eff} first increases rapidly and then reaches a constant value asymptotically. It should be noted that when a 100×100 mesh is used n_{eff} is accurate to 3rd decimal place, and the accuracy is increased to 4th decimal place when mesh size is increased to 500×500. A powerful extrapolation technique [21] was used to test the accuracy of modal solution for this nanowire structure. Aitken's procedure [21] extrapolates from three successive values of n_{eff} with a fixed geometric mesh division ratio in both the transverse dimensions of a waveguide:

$$n_{\text{eff}}^{\infty} = n_{\text{eff}(r+1)} - \frac{[n_{\text{eff}(r+1)} - n_{\text{eff}(r)}]^2}{n_{\text{eff}(r+1)} - 2n_{\text{eff}(r)} + n_{\text{eff}(r-1)}}, \tag{6}$$

We have plotted the extrapolated values of n_{eff}^{∞} in Fig. 1 by a red-dashed line. Using Eq. (6), for instance, we calculate Aitken's value from three n_{eff} values of 2.20901, 2.21377, and 2.21503 for $N = 50$, 100, and 200, respectively. From these three values, the extrapolated more accurate value is 2.21548. It is possible to get similar accuracy without using Aitken's extrapolation, but it would take a mesh finer than 1000×1000 to get it. Figure 1 clearly illustrates the convergence of raw FEM results and the advantage of using an extrapolation technique.

The GVD parameter, $D(\lambda) = -\frac{\lambda}{c}\frac{d^2 n_{\text{eff}}}{d\lambda^2}$ (ps/nm/km), is calculated numerically from the effective index obtained with FE method. Accuracy of the resulting curve is shown in Fig. 2 for three different mesh sizes for the same nanowire structure with $W = 700$ nm, $H = 500$ nm. The resulting dispersion curves nearly overlap since they are related to changes in the n_{eff} values rather than their absolute values. At the 1550 nm wavelength, GVD for three different meshes are calculated as 29.60 ps/nm/km, 30.49 ps/nm/km, and 30.94 ps/nm/km, respectively.

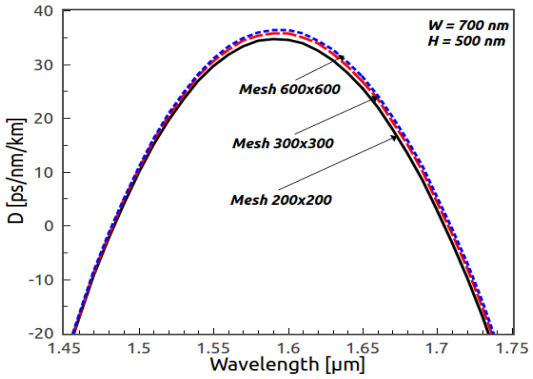

Fig. 2. GVD for the fundamental quasi-TE mode as a function of wavelength for the naowire structure with W = 700 nm and H = 500 nm. The black-solid, red-dashed, and blue-dotted correspond to a mesh size of 200×200, 300×300, and 600×600, respectively.

The small differences among these dispersion values do not result in significant changes in the SC spectrum. However, we have observed through numerical simulations that the third and higher-order dispersion parameters have significant effect on the SC generation. In the following numerical results we have used an appropriate mesh size and we are confident about the accuracy of numerically simulated results.

Next, to realize a ZDW close to the pump wavelength and to make dispersion slightly anomalous at this pump wavelength, we vary the dimension of $Ge_{11.5}As_{24}Se_{64.5}$ nanowires. In one set, thickness of the waveguide is kept constant at 500 nm and its width is varied as shown in Fig. 3(a). This figure shows dispersion curves having two ZDWs, with anomalous dispersion between these two ZDWs but both the peak value and slope of these curves increases as the width is increased. It can be observed from this figure that the 1st ZDW point with a positive slope shifts from left to right, and the 2nd ZDW with a negative slope also shift towards right but with a larger margin when W is increased. In this case the overall anomalous range also increases. Figure 3(a) clearly illustrates that the ZDW of the waveguide can be realized close to the pump wavelength by varying the width of that waveguide. In the other set of dispersion curves shown in Fig. 3(b), thickness of the waveguide is varied while keeping its width constant at 700 nm. In this case, ZDWs shift in the opposite directions, but the long one shifts more than the shorter one. It can be observed that the peak value of D increases when H is increased. Figures 3(a) and 3(b) indicate that the lower ZDW of a waveguide can be made to fall near the pump wavelength by adjusting the waveguide dimensions W and H.

To study SC generation one can solve Eq. (1) either in the time domain or in the frequency domain. We have tested both approaches, and they yield similar results. In this work, we have used time-domain formulation for our simulations using a split-step Fourier method, as this is the most commonly reported approach. Initially a waveguide with W = 700 nm and H = 500 nm is considered for SC generation. This nanowire structure is selected because the GVD of this structure is nearly flat near the pump wavelength of 1550 nm. Higher-order dispersion coefficients β_m ($m \geq 2$) upto eighth-order (β_2 to β_8) were calculated numerically from the dispersion curve. Our aim here is to study the effect of higher-order dispersion coefficients β_m ($m \geq 2$) terms on the supercontinuum bandwidth, and how the numerically simulated SC spectrum is modified with the inclusion of successive higher-order dispersion terms. Using the FE mode-solver, we obtain $A_{\text{eff}} = 0.28\ \mu\text{m}^2$ for our nanowire and this A_{eff} yields $\gamma = 123$ /W/m. For numerical simulations a TE polarized 50 fs FWHM secant pulse is launched with the peak power of 25 W. We include wavelength independent propagation loss of 3.2 dB/cm [13] for the

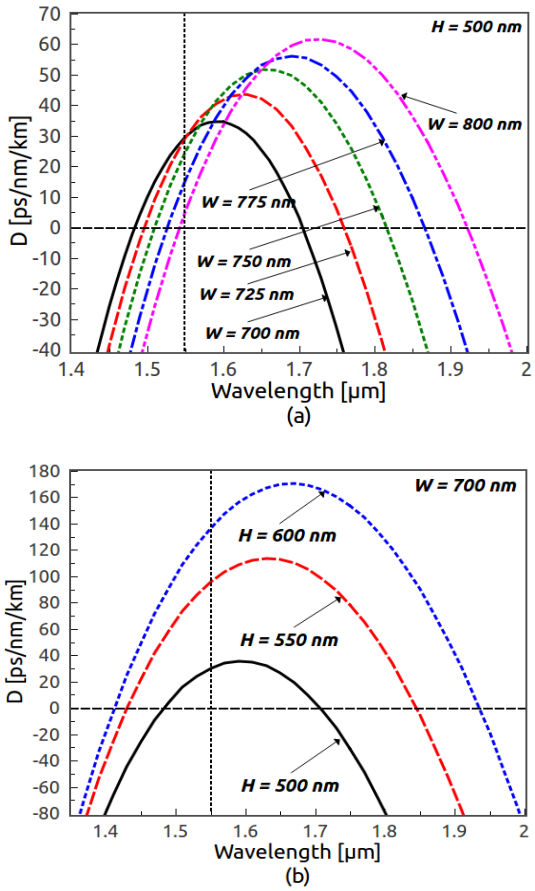

Fig. 3. GVD curves for the fundamental quasi-TE mode calculated from the n_{eff} values for (a) different W and same H and (b) different H and same W. Vertical dotted line represents the wavelength λ = 1550 nm.

18 mm long nanowire. Simulations have been carried out to test the effect of each higher-order dispersion (β_3 to β_8) terms successively and the generated spectra are shown in Fig. 4. With the addition of third-order dispersion term, the SC broadens from 850 nm to 3550 nm (black curve) resulting in a -60 dB bandwidth of around 2700 nm. The equivalent -20 dB bandwidth for this case is 1500 nm. However, after the addition of the fourth and other higher-order dispersion coefficients, the SC spectrum becomes narrower. Spectral narrowing converges slowly with the further addition of higher-order dispersion terms, and the spectra with β_m upto 7th and 8th terms are almost identical. For our nanowire structure the final supercontinuum extends from 1200 nm to 2100 nm.

Another set of results for the same nanowire structure (W = 700 nm and H = 500 nm) is shown in Fig. 5. As the pump lies in the anomalous GVD regime, SC generation is mainly dominated by the soliton fission process. For the soliton order, $\mathbb{N}$ = 8.13, soliton fission occurs at a distance of L_{fiss} = 2.6 mm, mainly because of perturbation induced by third and higher-order dispersions. To understand the spectrum broadening process we have considered terms upto β_3, β_4, and β_8 separately in this figure. When only third-order dispersion is added, multiple fundamental solitons are produced after the fission, whose spectra shift toward the longer

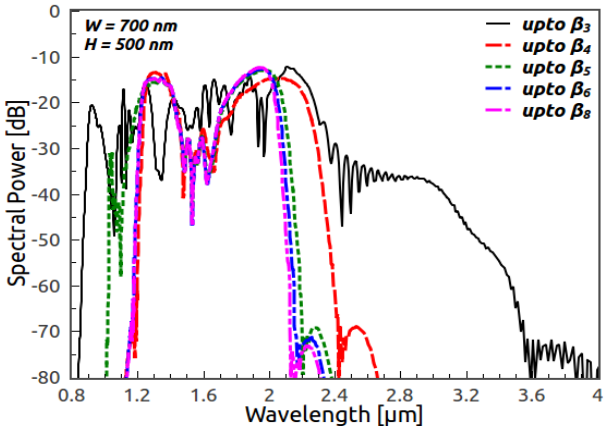

Fig. 4. Changes in SC spectra with the successive addition of higher-order dispersion terms for the nanowire of dimensions W = 700 nm and H = 500 nm.

wavelength side (stoke-side) because of intrapulse Raman scattering, producing multiple spectral peaks in the spectrum. In addition, non-solitonic radiation (NSR) in the form of dispersive wave is also generated but its spectrum lies on the shorter wavelength side (anti-stokes) of the input spectrum. When even-order dispersions such as β_4, β_8 terms are added, it is well-known that NSR is generated on both sides of the input spectrum. It is evident from Fig. 5 that the final SC depends strongly on how many dispersion terms are included, and one should include dispersion as accurately as possible to avoid spurious results.

To show sensitivity to the waveguide geometry, we consider another nanowire structure with W = 775 nm and H = 500 nm, having its ZDW closer to the pump wavelength compared to the previous structure. For this waveguide, with $A_{\text{eff}} = 0.31\ \mu\text{m}^2$ obtained by the FE technique, $\gamma =$

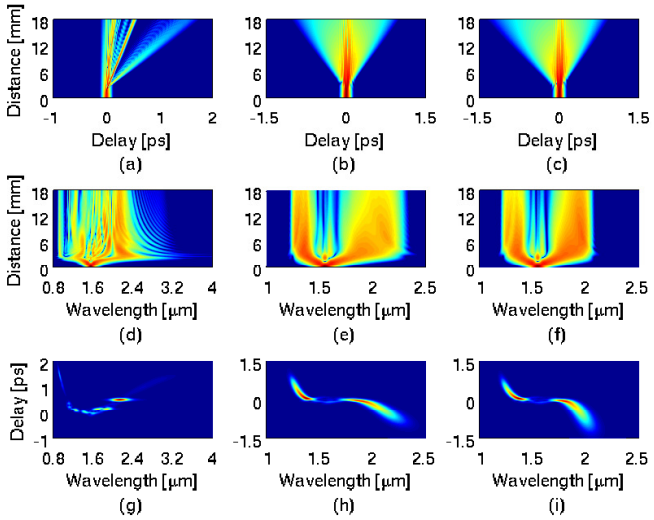

Fig. 5. Temporal intensity (top), spectral density (middle) and spectrogram (bottom) including terms upto β_3 (left column), upto β_4 (middle column), and upto β_8 (right column).

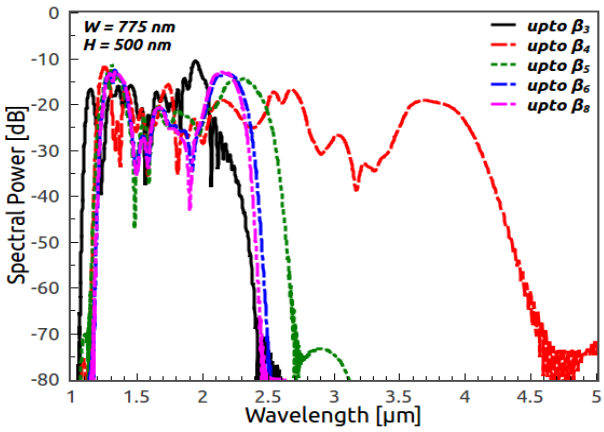

Fig. 6. Same as Fig.4 except for a different nanowire with W = 775 nm and H = 500 nm.

114 /W/m. After evaluating various dispersion coefficients from dispersion curve and keeping all other parameters the same, we have performed numerical simulations for dispersion terms upto β_8 successively. Figure 6 shows the resulting SC spectra and should be compared to Fig. 4. Unlike the previous structure interestingly we observe for this nanowire that SC spectrum gets broaden significantly when the β_4 term is added. However, after the addition of fifth and higher-order dispersion terms, SC spectrum again starts to become narrower. In this case, the SC extends from 1200 nm to 2400 nm when third-order dispersion in included, yielding a bandwidth of 1200 nm (1100 nm bandwidth at -20 dB). However, when fourth-order dispersion is added, the SC spectrum broadens upto 4600 nm generating bandwidth of 3400 nm (2950 nm bandwidth at -20 dB). On the other hand, with the addition of fifth and higher-order dispersion terms, spectrum becomes narrower. With the addition of β_8 term, the SC converges and has

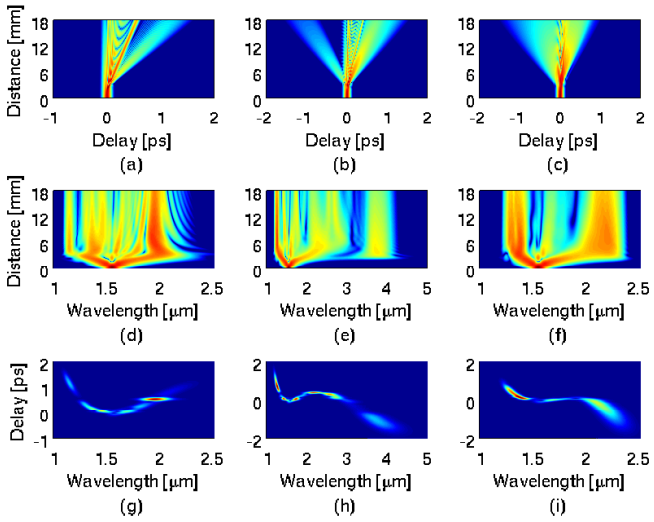

Fig. 7. Same as Fig. 5 except for a different nanowire with W = 775 nm and H = 500 nm.

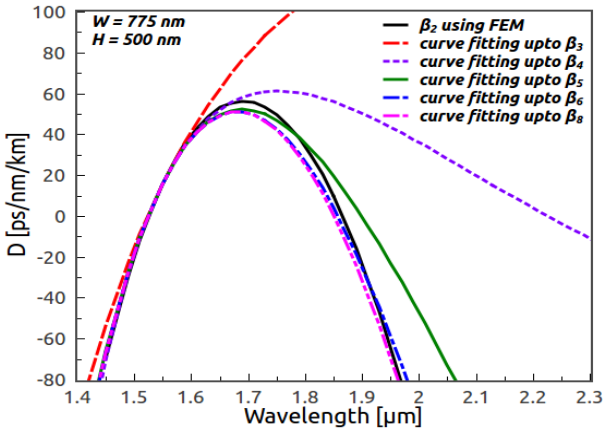

Fig. 8. Dispersion curve obtained with FE method (black) fitted the Taylor expansion upto β_8 for the nanowire W = 775 nm and H = 500 nm.

a final bandwidth of 1200 nm (1150 nm bandwidth at -20 dB). Spectrum obtained with upto β_7 term is not shown in Fig. 6 as this is almost identical to that of upto the β_8 term. The spectrograms and density plots corresponding to Fig. 6 are shown in Fig. 7. For the soliton order, $\mathbb{N}$ = 10.74 and the soliton fission length, L_{fiss} = 3.8 mm, the same phenomena occur after the addition of third-order dispersion. When the β_4 term is added, the Raman induced frequency shift (RIFS) reduces gradually as solitons spectra shift towards the second ZDW located at 1865 nm. Since β_3 is positive near the first ZDW but becomes negative near the second ZDW, the change in sign of β_3 changes the frequency associated with NSR generated during soliton fission and the RIFS is completely suppressed near the second ZDW. This phenomena has been called the spectral recoil effect [24,25]. According to energy conservation, as RIFS stops at the second ZDW, because of the spectral recoil effect soliton loses its energy to NSR that is red-shifted and lies in the infrared region beyond the second ZDW. The red-shifted NSR is mainly responsible for generating much larger SC bandwidth after addition of the β_4 term. This is also evident from spectral density and spectrogram shown in Figs. 7(e) and 7(h), respectively. This large SC bandwidth reduces considerably after addition of β_5 and higher-order terms. Once again, we note that a premature truncation of the Taylor series can lead to spurious and misleading results.

It should be noted that the dispersion of a waveguide is a strong function of the operating wavelength, and its nature determines the extent of the SC generation. However, Eq. (3), uses β_m values at the central frequency ω_0. By taking adequate number of higher-order terms one hopes to mimic the actual wavelength dependent $D(\lambda)$, but when a limited number of β_m terms are used, the resulting dispersion curve may be very different than the actual one. To confirm the accuracy of the GVD coefficients obtained from the FE mode-solver, we plot in Fig. 8 the GVD curves for the nanowire structure W = 775 nm, H = 500 nm obtained with the curve fitting method, using the Taylor series expansion and adding successively higher-order dispersion terms. However, as shown in Fig. 2, wavelength dependent dispersion $D(\lambda)$ can also be directly calculated over the whole wavelength range; this curve is shown by a black line in Fig. 8. It is apparent from the figure that the GVD curve obtained from curve fitting closely matches with the actual GVD when dispersion upto eighth-order is included. This gives us confidence in claiming that the results obtained by truncating the Taylor series at the β_8 term represent the situation one will observe in actual experiments.

To study the impact of device geometry, we have carried out rigorous simulations for multiple

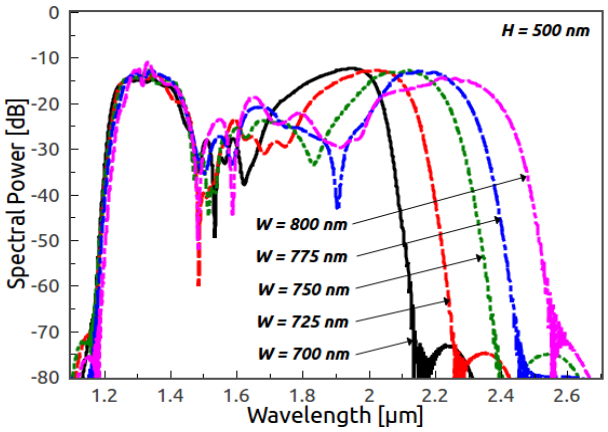

Fig. 9. Numerically simulated SC spectra for nanowires with the dispersion curves shown in Fig. 3 by including dispersion terms upto β_8.

GeAsSe planar structures whose width varies from 700 to 800 nm, and some of the results were shown in Fig. 9. For this set, their GVD curves are shown in Fig. 3(a). Dispersion coefficients upto β_8 term included for all simulations shown in Fig. 9. For the nanowire structure with W = 800 nm, H = 500 nm which has its ZDW very close to the pump wavelength, it can be observed from Fig. 9 that the SC extends over 1300 nm (1250 nm bandwidth at -20 dB) covering a wavelength range from 1200 nm to 2500 nm, which is more than the bandwidth achieved by other nanowire structures with widths less than 800 nm.

4. Conclusions

To take advantage of dispersion engineering, the $Ge_{11.5}As_{24}Se_{64.5}$ nanowire can be designed in such a way that it exhibits anomalous dispersion near a chosen pump wavelength and generates broadband supercontinuum at low pump powers in the form of a compact device. As numerically generated SC spectra critically depends on the dispersion properties of the nanowire waveguide, we have also discussed how the accuracy of dispersion is affected with the choice of the mesh size used for the FE technique. We have numerically studied SC generation in such nanowires by dispersion engineering and discussed the effects of higher-order dispersion coefficients from β_3 to β_8 terms on their SC bandwidths. We have considered five nanowire structures with widths in the range of 700 to 800 nm (same 500 nm thickness). As shown in Fig. 3(a), that all five of them exhibit anomalous dispersion at a pump wavelength of 1550 nm and all have two ZDWs. We have carried out numerical simulations for all five nanowire structures and optimized the design to realize a wider bandwidth for SC generation. In Ref. [1, 2, 27] it is recommended to use $\beta(\omega) - \beta(\omega_0) - \beta_1(\omega_0)(\omega - \omega_0)$ instead of $\beta_m(\omega) = \frac{d^m\beta}{d\omega^m}\big|_{\omega=\omega_0}$ $(m \geq 2)$ for calculating the total dispersions. To implement dispersion using the first approach, one needs to know the propagation constant $\beta(\omega)$ over the whole frequency range of the supercontinuum. This approach may not appropriate for microstructured fibers with air holes within its cladding [2]. The second approach is often used because it is easier to determine higher-order dispersion parameters at a particular wavelength using the Taylor series expansion and one does not need to know about $\beta(\omega)$ over the whole SC bandwidth. Our work highlights the effects of higher-order dispersion coefficients on the SC spectrum and identifies changes that occur with addition of each successive dispersion coefficient in numerical simulations. In earlier simulation-based works on SC generation, sometimes the Taylor series expansion has been

truncated after the third-order or fourth-order term. We have shown that this may not produce an accurate SC spectrum and more higher-order dispersion terms may need to be included to obtain a reliable SC spectrum. In our work propagation losses for nanowires were taken to be 3.2 dB/cm [13]. Recent work has shown that this can be reduced to around 1.5 dB/cm through process improvements [14]. Our conclusions are not affected if this lower value of loss is used for simulations. Finally several GeAsSe structures are studied, and one optimized structure, with W = 800 nm and H = 500 nm, shows that large bandwidth of SC using chalcogenide nanowires is possible.